Efficiency and Accuracy of the Klemp–Wilhelmson Time-Splitting Technique

WILLIAM C. SKAMAROCK AND JOSEPH B. KLEMP

National Center for Atmospheric Research, Boulder, Colorado*

27 May 1994 and 10 June 1994

1. Introduction

In atmospheric simulations using both the hydrostatic and nonhydrostatic equations, modes of physical interest often are of much lower frequency than the highest-frequency modes admitted by the equations, such as high-frequency gravity and acoustic modes, that are meteorologically unimportant. Numerical techniques used to integrate the equations are often time-step limited by these irrelevant modes, and a popular integration approach is to integrate the high-frequency components with a smaller time step, or with an implicit technique, while integrating the lower-frequency components with an explicit scheme and an appropriately longer (and more economical) time step. Klemp and Wilhelmson (1978, hereafter KW) introduced a technique for integrating the compressible nonhydrostatic equations using a large time step with the leapfrog time-integration scheme for the low-frequency modes, and a small time step with the forward–backward scheme of Mesinger (1977) for integrating the terms responsible for the horizontally propagating acoustic modes together with an implicit scheme for integrated the vertically propagating acoustic modes. Tatsumi (1983) independently developed essentially the same technique for treating the horizontally propagating gravity wave modes in a hydrostatic primitive equation model. Skamarock and Klemp (1992, hereafter SK) analyzed the stability of this and other techniques and concluded that the KW method appears to offer the best combination of stability, minimal filtering, simplicity, and freedom from spurious noise for integrating the hydrostatic or nonhydrostatic equations.

When choosing a splitting scheme, accuracy and efficiency are also important factors that must be considered. Skamarock and Klemp did not quantify the efficiency or the accuracy of the KW method compared to the fully explicit nonsplit leapfrog technique. In this note, we show that the KW scheme is both efficient and accurate for integrating the nonhydrostatic compressible equations both for grids with vertical to horizontal aspect ratio ($\Delta z/\Delta x$) $\sim$ 1 and for aspect ratios much less than 1. We also comment on the accuracy of the integration of the nonhydrostatic equations at hydrostatic scales, where several research groups have shown that the nonhydrostatic equations can be integrated as efficiently as the hydrostatic equations using both semi-implicit and KW-type integration techniques (e.g., Tanguay et al. 1990; Cullen 1990; Dudhia 1993).

Browning and Kreiss (1994) have suggested that the KW scheme is no more efficient (and possibly much more costly) than the fully explicit leapfrog scheme and may be highly inaccurate in certain applications, and they suggest the use of an alternative equation set, proposed by Browning and Kreiss (1986), for simulating all scales of atmospheric motion. We demonstrate that the alternative set is highly inaccurate for nearly hydrostatic inertia–gravity waves and, therefore, is not appropriate for most mesoscale and many larger-scale applications.

2. The methods

To demonstrate the efficiency and accuracy of the KW method for integrating the nonhydrostatic equations, we examine a simplified two-dimensional Boussinesq equation set:

$$\frac{\partial u}{\partial t} + \frac{\partial \pi}{\partial x} = -u\frac{\partial u}{\partial x} - w\frac{\partial u}{\partial z} + fv \tag{1}$$

$$\frac{\partial v}{\partial t} = -u\frac{\partial v}{\partial x} - w\frac{\partial v}{\partial z} - fu \tag{2}$$

$$\frac{\partial w}{\partial t} + \frac{\partial \pi}{\partial z} = g\left(\frac{\theta}{\bar{\theta}} - 1\right) - u\frac{\partial w}{\partial x} - w\frac{\partial w}{\partial z} \tag{3}$$

$$\frac{\partial \pi}{\partial t} + c_s^2\left(\frac{\partial u}{\partial x} + \frac{\partial w}{\partial z}\right) = -u\frac{\partial \pi}{\partial x} - w\frac{\partial \pi}{\partial z} \tag{4}$$

$$\frac{\partial \theta}{\partial t} = -u\frac{\partial \theta}{\partial x} - w\frac{\partial \theta}{\partial z}. \tag{5}$$

Equations (1)–(5) are the horizontal and vertical momentum, pressure, and thermodynamic equations, respectively; u, v, and w are the fluid velocities in x, y,

* The National Center for Atmospheric Research is sponsored by the National Science Foundation.

Corresponding author address: William C. Skamarock, NCAR, P.O. Box 3000, Boulder, CO 80307-3000.

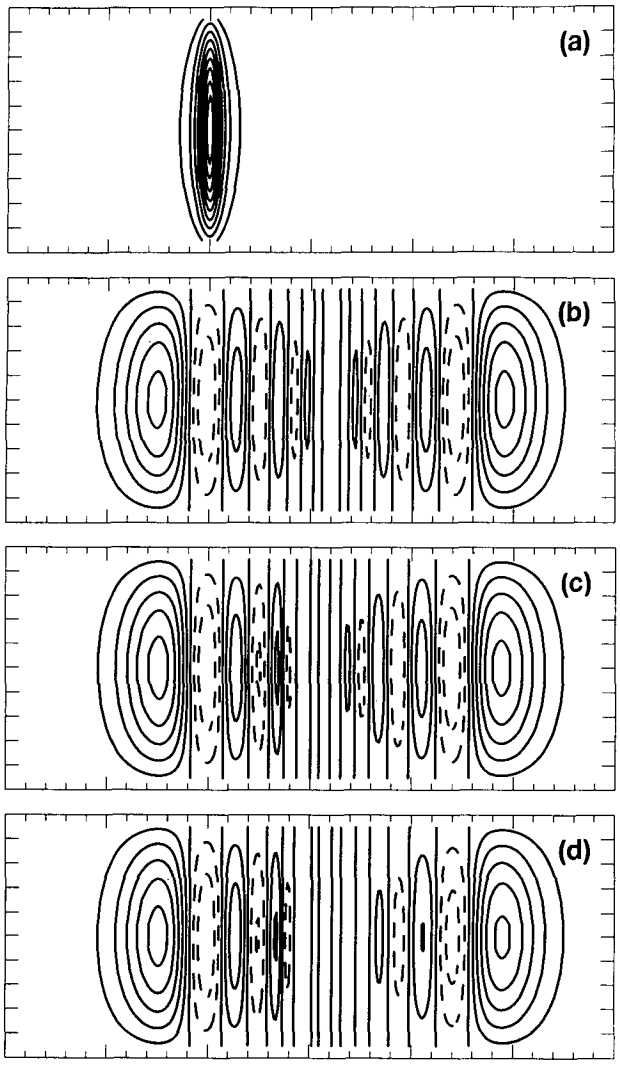

FIG. 1. (a) Perturbation θ at $t = 0$ for the nonhydrostatic gravity wave tests, plotted with a contour interval of 10^{-3} K. The plotted domain is 300 km × 10 km. The perturbation θ at $t = 3000$ s, plotted with a contour interval of 0.5×10^{-3} K, for (b) the analytic solution, (c) the fully explicit model with $\Delta t = 1$ s, and (d) the semi-implicit KW model with $\Delta t = 12$ s. Negative contours are dashed.

and z; θ is the potential temperature; $\bar{\theta}(z)$ is the mean potential temperature; π is a perturbation pressure [$\Pi = \bar{\Pi} + \pi = c_p\theta_0(p/p_0)^{R/c_p}$]; g is the gravitational constant; t is time; and c_s is the speed of sound. This system is appropriate for shallow convection (Ogura and Phillips 1962) and is a Boussinesq system except that we have retained compressibility for computational convenience. While we use this simple equation set to facilitate direct comparison of numerical solutions with analytic solutions, the numerical methods we consider apply directly to the fully compressible Navier–Stokes equations.

We concern ourselves with discretizations on the C grid, which is used in many nonhydrostatic and hydrostatic models. Although the computation of advection terms is more expensive on the C grid than on a nonstaggered grid, the C grid has the advantage of accurately resolving the gravity wave modes (Haltiner and Williams 1980, p. 227). Defining averaging and differencing operators,

$$\bar{\phi}^{\xi} = \frac{1}{2}(\phi_{\xi+\Delta\xi/2} + \phi_{\xi-\Delta\xi/2})$$

and

$$\delta_{\xi}\phi = \frac{1}{\Delta\xi}(\phi_{\xi+\Delta\xi/2} - \phi_{\xi-\Delta\xi/2}),$$

a fully explicit leapfrog discretization of (1)–(5) is

$$u^{t+\Delta t} = u^{t-\Delta t} - 2\Delta t(\delta_x\pi^t - F_u^t) \tag{6}$$

$$v^{t+\Delta t} = v^{t-\Delta t} + 2\Delta t F_v^t \tag{7}$$

$$w^{t+\Delta t} = w^{t-\Delta t} - 2\Delta t(\delta_z\pi^t - F_w^t) \tag{8}$$

$$\pi^{t+\Delta t} = \pi^{t-\Delta t} - 2\Delta t(c_s^2 D^t - F_\pi^t) \tag{9}$$

$$\theta^{t+\Delta t} = \theta^{t-\Delta t} + 2\Delta t F_\theta^t, \tag{10}$$

where

$$F_u = -\overline{\bar{u}^x \delta_x u}^x - \overline{\bar{w}^x \delta_z u}^z + f\bar{v}^x$$

$$F_v = -\overline{u\delta_x v}^x - \overline{w\delta_z v}^z - f\bar{u}^x$$

$$F_w = -\overline{\bar{u}^z \delta_x w}^x - \overline{\bar{w}^z \delta_z w}^z + \frac{g}{\bar{\theta}}\overline{(\theta^t - \bar{\theta})}^z$$

$$F_\pi = -\overline{u\delta_x\pi}^x - \overline{w\delta_z\pi}^z$$

$$F_\theta = -\overline{u\delta_x\theta}^x - \overline{w\delta_z\theta}^z$$

and

$$D = \delta_x u + \delta_z w.$$

The terms F_u, F_v, F_w, F_π, and F_θ, on the right-hand sides of (6)–(10), are evaluated at time t. Leapfrog-based models also include a time filter analyzed by Robert (1966).

The KW method advances the continuous set (1)–(5) from t to $t + \Delta t$ by integrating the discretized momentum and pressure equations

$$u^{\tau+\Delta\tau} = u^\tau - \Delta\tau(-\delta_x\pi^\tau - \alpha_d D_x^\tau - F_u^t) \tag{11}$$

$$w^{\tau+\Delta\tau} = w^\tau - \Delta\tau(\delta_z\pi^\tau - \alpha_d D_z^\tau - F_w^t) \tag{12}$$

$$\pi^{\tau+\Delta\tau} = \pi^\tau - \Delta\tau(c_s^2 D^{\tau+\Delta\tau} - F_\pi^t) \tag{13}$$

from $t - \Delta t$ to $t + \Delta t$ (over the leapfrog step) using several small time step $\Delta\tau$ and holding the rhs terms F_u, F_w, and F_π fixed at time t over these small time steps. Equations (11)–(13) are called the "small-time-step equations," and $\Delta\tau$ is chosen so as to be stable for the acoustic-mode integration, where typically $\Delta\tau$ is 2–10, or more, times smaller than Δt (chosen so as to be stable for advection and gravity modes),

depending on the application. The terms responsible for the acoustic modes, on the lhs of (1), (3), and (4), are active in these small time steps, while the low-frequency terms, including all advection, buoyancy, and Coriolis terms [the rhs terms in (1), (3), and (4)], are fixed. The remaining continuous equations, (2) and (5), are discretized as in the explicit leapfrog scheme and are stepped forward only on the large time step using (7) and (10). Thus, the integration procedure is to step forward the large time-step equations (7) and (10) (for the acoustically inactive variables), evaluate the rhs terms F_u^t, F_w^t, and F_p^t, and advance equations (11)–(13) from $t - \Delta t$ to $t + \Delta t$ using $n_s = 2(\Delta t/\Delta\tau)$ time steps. Finally, to control the weak instability analyzed by SK for this splitting scheme, divergence damping terms are included [these are the terms multiplied by α_d in (11) and (12); see SK for details]. Divergence damping does not compromise the accuracy of the modes of physical interest since it damps only the physically unimportant acoustic modes.

First, we emphasize that by using forward–backward differencing on the horizontal pressure and divergence terms in (11) and (13) (KW; Mesinger 1977), only half as many time steps are required because the advection terms are removed from the small time-step calculations. This occurs because without the advection terms no terms need be evaluated at the middle time level [$\tau + 1/2\Delta\tau$ in (11)–(13)] in a leapfrog time step. Since the even and odd time steps are then totally decoupled, the time stepping for the small time steps can advance using only the even levels, and this procedure produces results identical to the full leapfrog scheme but with only half the calculations. The use of the forward–backward scheme in a fully explicit leapfrog model does not result in any efficiency gain, because the slow-frequency terms must be evaluated at the midpoint of the time step.

For grids with an aspect ratio ($\Delta z/\Delta x$) significantly less than 1, the efficiency of the KW scheme is increased by using an implicit time discretization for the terms responsible for vertically propagating acoustic modes. In this case, (12) and (13) are replaced by

$$w^{\tau+\Delta\tau} = w^{\tau} - \Delta\tau\left[\frac{1}{2}(\delta_z\pi^{\tau} + \delta_z\pi^{\tau+\Delta\tau}) - \alpha D_z - F_w^t\right] \tag{14}$$

$$\pi^{\tau+\Delta\tau} = \pi^{\tau} - \Delta\tau\left[c_s^2\delta_x u^{\tau+\Delta\tau} + \frac{c_s^2}{2}(\delta_z w^{\tau} + \delta_z w^{\tau+\Delta\tau}) - F_{\pi}^t\right]. \tag{15}$$

3. Efficiency and accuracy of the KW scheme

To demonstrate the efficiency and accuracy of the KW scheme, we have simulated a propagating inertia–gravity wave in a Boussinesq atmosphere of constant Brunt–Väisälä frequency $N = 10^{-2}\ \mathrm{s}^{-1}$, in a periodic channel of length L with solid, free-slip upper and lower boundaries at $z = 0, H$. The waves are excited by an initial θ perturbation of the form

$$\theta(x, z, 0) = \Delta\theta_0 \frac{\sin(\pi z/H)}{1 + (x - x_c)^2/a^2}, \tag{16}$$

and a small amplitude initial perturbation, $\Delta\theta_0 = 10^{-2}$, is used to facilitate quantitative comparisons with analytic solutions of the linearized equations

$$u_t + Uu_x + \pi_x = fv \tag{17}$$

$$v_t + Uv_x = -fu \tag{18}$$

$$w_t + Uw_x + \pi_z - \frac{g\theta}{\theta_0} = 0 \tag{19}$$

$$\theta_t + U\theta_x + \left(\frac{\theta_0}{g}\right)N^2 w = 0 \tag{20}$$

$$\pi_t + U\pi_x + c_s^2(u_x + w_z) = 0. \tag{21}$$

Ignoring the acoustic modes, (21) may be approximated by $u_x + w_z = 0$, in which case the solution to these equations, subject to the initial condition (16), is given by

$$\theta(\tilde{x}, z, t) = \theta(\tilde{x}, z, 0) + \Delta\theta_0 a \sin(lz) \times \int_0^{\infty} \frac{k^2N^2}{k^2N^2 + l^2f^2} \exp(-ak)(\cos\lambda t - 1)\cos k\tilde{x}\, dk, \tag{22}$$

where $l = \pi/H$, $\tilde{x} = x - Ut$ reflects the translation of the x-coordinate framework due to the mean advection velocity U, and

$$\lambda^2 = \frac{k^2N^2 + l^2f^2}{k^2 + l^2}. \tag{23}$$

First, consider the case of a grid with an aspect ratio ($\Delta z/\Delta x$) = 1. Figure 1 shows the solutions at t = 3000 s of the linear analytic model, the fully explicit leapfrog model, and the KW semi-implicit model [the KW semi-implicit and KW explicit (not shown) models give almost identical solutions]. The simulations use a channel of length L = 300 km and H = 10 km, Δx = Δz = 1 km, a perturbation half-width a = 5 km, c_s = 300 m s^{-1}, and U = 20 m s^{-1}. The parameters for the model runs, along with timing and efficiency statistics, are given in Table 1. The 1-s time step for the fully explicit leapfrog method is slightly less than the maximum allowable ($\Delta t \approx \leq \Delta x/2\sqrt{2}c_s$). The small time step for the split-explicit KW model is twice the explicit model time step ($\Delta\tau$ = 2 s) because the KW model uses the forward–backward scheme. The small time step for the semi-implicit KW model is not constrained by the vertically propagating acoustic waves; hence, it is larger by approximately a factor of $\sqrt{2}$ ($\Delta\tau$

TABLE 1. Efficiency statistics for the split-implicit KW, split-explicit KW, and fully explicit leapfrog models, for the nonhydrostatic simulation ($\Delta x/\Delta z = 1$, $T = 3000$ s).

	Split implicit	Split explicit	Explicit
Parameters			
Δt (large) (s)	12	12	1
$\Delta\tau$ (small) (s)	3	2	—
Steps (large)	250	250	3000
Steps (small)	2000	3000	—
Timings (CPU s)			
Large steps	5.51	5.47	70.56
Small steps	15.52	13.47	—
Total	20.76	18.94	70.56
CPU(s) per step			
Large step	2.20×10^{-2}	2.18×10^{-2}	2.35×10^{-2}
Small step	7.62×10^{-3}	6.31×10^{-3}	—
FLOPS per step per point			
Large step	104	104	112
Small step	39	25	—
FLOPS per point			
Total for integration	1.04×10^5	1.01×10^5	3.36×10^5

$= 3$ s). The large time step Δt in the KW explicit and semi-implicit models is not constrained by the acoustic modes, and $\Delta t = 12$ s, appropriate for advection and gravity wave modes, is used. As revealed in Table 1, both KW models are faster than the fully explicit leapfrog model by approximately a factor of 3. Surprisingly, the semi-implicit KW model realizes this efficiency gain because the extra overhead of solving the tridiagonal system for each column is offset by the larger small time step allowed with its use. The data in Table 1 also reveal that the operation counts for the schemes are a reasonable predictor of their cost in an actual computation.[1]

The accuracy of the schemes is qualitatively revealed in comparative solutions in Fig. 1. The fully explicit and semi-implicit KW models have a mean Courant number for advection of $U\Delta t/\Delta x = 0.02$ and 0.24, respectively. Note that there are small errors in both simulations compared with the analytic solution but that the errors are similar; hence, it is the spatial resolution that is limiting the solution accuracy and not the temporal resolution. Also note that the symmetry in the analytic solution is not maintained in any of the numerical solutions; phase errors arising from the advection scheme produce the asymmetry. Figure 2 shows the time evolution of the normalized rms errors for the simulations. The errors for the splitting schemes and for the fully explicit leapfrog scheme are similar, and further investigation reveals that the slight increase in the explicit model error is due to the fact that the larger temporal error in the split schemes may be canceling some of the spatial error, as opposed to increasing the overall error, although this cannot be expected in other cases. Also shown in Fig. 2 is the error for the semi-implicit KW model using a large time step of 30 s ($U\Delta t/\Delta x = 0.6$). Here the errors are significantly larger, because the errors from the time integration scheme are beginning to dominate those from the spatial discretization.

The preceding results demonstrating the efficiency and accuracy of the KW time-splitting technique contradict those of Browning and Kreiss (1994). We believe the primary reasons for this contradiction are our use of a staggered grid (in which the advection terms are computationally more expensive than on a nonstaggered grid) and our efficient coding of the small-time-step algorithm (which takes advantage of the odd–even time-step decoupling in the small time steps as described in the previous section).

Next, consider the case of a smaller aspect-ratio grid. In this case the simulations use a channel of length $L = 6000$ km and $H = 10$ km, $\Delta x = 20$ km and $\Delta z = 1$ km, a perturbation half-width $a = 100$ km, $c_s = 300$ m s^{-1}, and $U = 20$ m s^{-1}. The analytic solution, the solution using the semi-implicit KW model, and a hydrostatic model solution are shown at 60 000 s in Fig. 3. The semi-implicit model uses a 200-s large time step, an advection Courant number of 0.2, and a 40-s small time step, resulting in a CPU time of approximately 29.3 s. Thus, while we have increased the horizontal scale and the simulation time by a factor of 20 over the

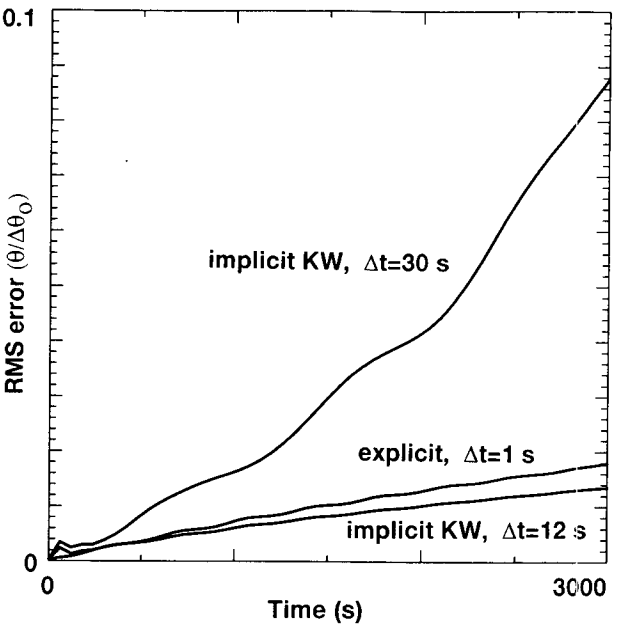

FIG. 2. Normalized rms errors for the nonhydrostatic simulations.

[1] The simulations were performed on an SGI R4000 workstation, and the relative efficiencies are similar on DEC Alpha/5000 and IBM 590 workstations.

previous problem, the simulation takes a similar amount of CPU time because it is not limited by the vertically propagating sound waves. In the hydrostatic model, two vertical integrations of a continuity equation and an integration of a hydrostatic equation replace the small time steps and vertical momentum equation. However, the time step is reduced to 25 s since it is limited by the horizontally propagating acoustic modes, and the total integration CPU time is 54.4 s. For the split-explicit KW model and fully explicit leapfrog model (models that are time step limited by the vertically propagating acoustic modes), the CPU time would increase by a factor of approximately 15 over that in the previous simulations with a grid aspect ratio of unity. Thus, for grid aspect ratios significantly less than 1, the explicit methods are prohibitively expensive compared with the vertically semi-implicit schemes for compressible nonhydrostatic model applications. In practice, grid aspect ratios span a broad range in nonhydrostatic applications and often include selective reduction of the vertical grid length near the ground to better resolve boundary layer structure.

Other factors may alter the efficiency of the methods when implemented in a fully compressible cloud, mesoscale, or large-scale nonhydrostatic model. When moving from two to three dimensions, the costs of the advection terms increases relative to the acoustic terms because five new advection terms are added to the low-frequency terms, while a third short equation and only a single additional divergence calculation is added to the small-time-step equations. Moreover, the differencing used in the advection operators is quite simple in these examples, and more complex operators (with important numerical properties such as energy and enstrophy conservation, higher-order accuracy, etc.) are often used in application models. The small-time-step equations in the application models are very similar to what we have presented. Thus, overall, greater efficiency gains can often be obtained in the full models compared to the simpler models.

The accuracy of the nearly hydrostatic simulations using the semi-implicit KW model can be appreciated qualitatively by examining Fig. 3, and is quantitatively illustrated in Fig. 4, which depicts the normalized rms error for the semi-implicit KW model and for the hydrostatic model. The errors are comparable in magnitude to the models run at nonhydrostatic scale. Also shown in Fig. 4 is the solution error for an incompressible ($u_x + w_z = 0$) hydrostatic Boussinesq model that uses a 200-s time step. The lower error in the Boussinesq model indicates that a significant portion of the difference between the compressible KW model and analytic solutions may be a result of the KW model compressibility.

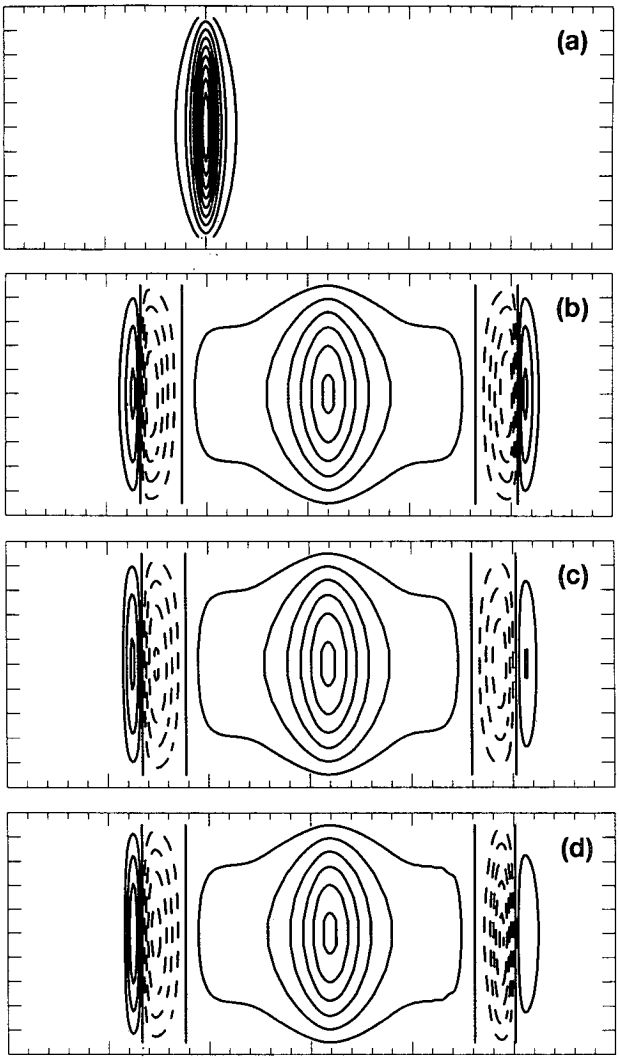

FIG. 3. (a) Perturbation θ at $t = 0$ for the hydrostatic gravity wave tests, plotted with a contour interval of 10^{-3} K. The plotted domain is 6000 km × 10 km. The perturbation θ at $t = 60\,000$ s, plotted with a contour interval of 0.5×10^{-3} K, for (b) the analytic solution, (c) the semi-implicit KW model with $\Delta t = 200$ s, and (d) the hydrostatic model. Negative contours are dashed.

4. Hydrostatic-scale simulations with nonhydrostatic models

For problems in which the horizontal length scale is much larger than the vertical length scale, the vertical sound speed becomes crippling to explicit schemes for solving the 3D Euler equations; this limitation provided the original motivation for using the primitive (hydrostatic) equations in numerical weather prediction models. However, as shown in the previous section, the nonhydrostatic Euler equations can also resolve the slow modes accurately and efficiently at large horizontal length scales by treating implicitly the terms responsible for vertical sound wave propagation.

The implicit differencing admittedly distorts the vertically propagating acoustic modes but does so in a manner that is not disruptive to the slower modes of physical interest. Consider semi-implicit differencing in the vertical for terms responsible for acoustic modes

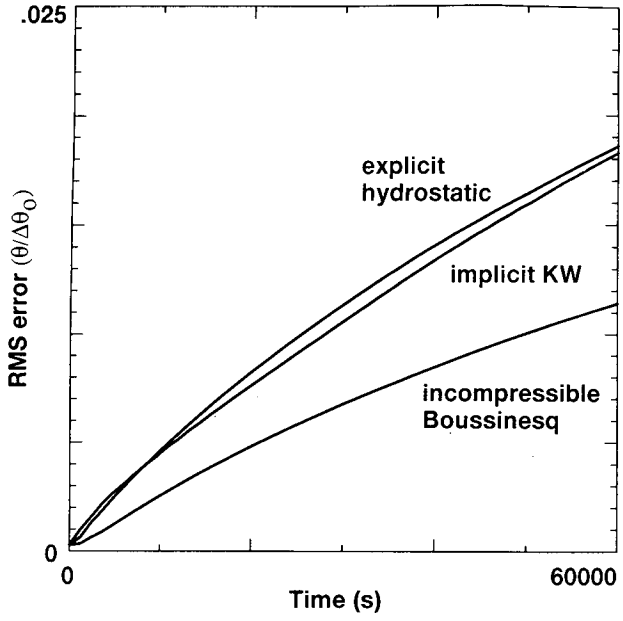

FIG. 4. Normalized rms errors for the hydrostatic simulations.

in the linearized equations (17)–(21), where leapfrog time differencing takes place between time levels $t - \Delta t$ and $t + \Delta t$, and Coriolis and advective effects ($f = 0$ and $U = 0$) are ignored. Assuming disturbances of the form $\exp[i(k_x x + k_z z - \omega t)]$ leads to the following dispersion equation for the semi-implicit differencing:

$$\sin^2\omega\Delta t = \frac{\lambda_x^2 + \lambda_z^2 + \beta^2 \pm [(\lambda_x^2 + \lambda_z^2 + \beta^2)^2 - 4\lambda_x^2(1 + \lambda_z^2)\beta^2]^{1/2}}{2(1 + \lambda_z^2)}, \quad (24)$$

where $\lambda_x = k_x c_s \Delta t$, $\lambda_z = k_z c_s \Delta t$, and $\beta = N\Delta t$. Here, we have assumed perfect resolution in the spatial derivatives; for specific finite differencing, the wavenumbers can be replaced by the appropriate approximation [that is, for second-order centered differencing, k_x would be replaced by $2\sin(k_x\Delta x/2)/\Delta x$]. Recognizing that the first term within the radical is much greater than the second yields

$$\frac{\sin\omega_a\Delta t}{\Delta t} \approx \pm\left[\frac{(k_x^2 + k_z^2)c_s^2 + N^2}{1 + \lambda_z^2}\right]^{1/2}, \quad (25)$$

and

$$\frac{\sin\omega_g\Delta t}{\Delta t} \approx \pm\left[\frac{k_x^2 N^2}{k_x^2 + k_z^2 + N^2/c_s^2}\right]^{1/2}. \quad (26)$$

Notice that no artificial amplification occurs (i.e., the frequencies remain real) in both the gravity wave (ω_g) and acoustic (ω_a) modes as long as the magnitudes of the rhs of (25) and (26) multiplied by Δt remain less than unity. The semi-implicit scheme has slowed the acoustic modes by the factor $1 + \lambda_z^2$ in the denominator of (25), but the gravity wave frequency has the same form as a fully explicit representation.

Browning and Kreiss (1994, hereafter BK) point out that for large differences between horizontal and vertical length scales (termed "badly skewed" by BK), "the semi-implicit approximation is equivalent to solving the primitive equations." We agree, and believe this is the correct limit for the Euler equations in the limit of large horizontal length scale. Moreover, BK suggest that because solutions to the Euler equations at large horizontal length scales behave like the primitive equations, they are ill posed in the presence of lateral boundaries in the integration domain [see Oliger and Sundström (1978) for a discussion of the ill posedness of the initial value problem]. To remedy this difficulty, BK advocate the use of an approximate equation set in which the fast modes are artificially slowed down (Browning and Kreiss 1986; BK; Browning and MacDonald 1993). This is accomplished by adding a parameter α that multiplies the pressure and buoyancy terms in the vertical momentum equation (i.e., the only terms that would be present if the system were hydrostatic). For example, the linear system (17)–(21) can be recast with the BK approximation by replacing (19) with

$$w_t + Uw_x + \alpha\left(\pi_z - \frac{g\theta}{\theta_0}\right) = 0. \quad (27)$$

By specifying the speed reduction factor α as the square of the aspect ratio (i.e., H^2/L^2 or $\Delta z^2/\Delta x^2$, where H and L are the vertical and horizontal length scales, respectively) the gravity wave modes are artificially altered such that they become nonhydrostatic, thereby removing the ill posedness of the hydrostatic modes in the presence of lateral boundaries. This is readily illustrated through the linear dispersion equation for inertia–gravity waves in the 3D Euler equations. Employing the same approach as used in deriving (25) and (26), the dispersion relation for the linear 2D differential equations, including the speed reduction factor α, the mean advection terms, and the Coriolis terms, yields

$$\omega_a \approx k_x U \pm [(k_x^2 + k_y^2 + \alpha k_z^2)c_s^2 + \alpha^2 N^2 + f^2]^{1/2} \quad (28)$$

$$\omega_g \approx k_x U \pm \left[\frac{(k_x^2 + k_y^2)N^2 + (k_z^2 + N^2/c_s^2)f^2}{\alpha^{-1}(k_x^2 + k_y^2) + k_z^2 + N^2/c_s^2}\right]^{1/2}. \quad (29)$$

Equation (29) recovers the proper dispersion relation for the gravity wave modes for $\alpha = 1$, in which case the hydrostatic response arises when the first term in the denominator becomes negligible as $k_x^2 + k_y^2 \ll k_z^2$. By specifying α as the square of the aspect ratio, the

acoustic frequency is reduced, and the gravity waves become artificially nonhydrostatic as the first term in the denominator of (29) becomes the same order as k_z^2.

The problem with this approach is that it cannot be used for any applications in which inertia–gravity waves are of physical interest or importance in the simulation, since specifying $\alpha \ll 1$ will produce first-order errors in gravity wave structure and propagation. For example, the evolving flow depicted in Fig. 3 is greatly distorted if the BK equation set is employed. This can be illustrated through the linear analytic solution obtained by using (27) instead of (19) to derive (22), which remains the same except

$$\lambda^2 = \frac{k^2N^2 + l^2f^2}{\alpha^{-1}k^2 + l^2} \tag{30}$$

replaces (23). Specifying $\alpha = (\Delta z/\Delta x)^2 = 2.5 \times 10^{-3}$ yields the structure shown in Fig. 5b, which bears little resemblance to the reference solution with $\alpha = 1$ (repeated in Fig. 5a). Physically, the inertia–gravity waves radiating outward from the initial perturbation are being artificially slowed, and consequently, the adjustment toward a geostrophically balanced flow (evident in the central portion of Fig. 5a) is significantly retarded.

Inertia–gravity waves are the primary means by which ageostrophic motions are realized, and frequently these waves are essentially hydrostatic in nature. For example, hydrostatic mountain waves are often the dominate modes contributing to the vertical transport of momentum (Lilly et al. 1982; Klemp and Lilly 1980). The impact of BK speed reduction on these large-scale mountain waves is particularly dramatic. This is illustrated from (29) for steady 2D flow (ignoring the small terms divided by c_s^2 and Coriolis forcing), which reduces to the well-known Scorer equation

$$k_z^2 = \frac{N^2}{U^2} - \frac{k_x^2}{\alpha}, \tag{31}$$

modified by α. For nearly hydrostatic modes, the second term in (31) is negligible and the vertical wavenumber for all k_x in the terrain forcing is just the Scorer parameter (N/U). However, if α is chosen to make the modes artificially nonhydrostatic, k_z will be significantly reduced. If α is specified as the square of the aspect ratio, the two terms on the rhs of (31) will have the same magnitude, causing the vertical wavelength to increase dramatically and, in regions where the second term might exceed the first, causing artificial ducting of the wave.

Mesoscale gravity waves also have been documented as the source of a variety of severe weather events (e.g., Stobie et al. 1983; Bosart and Seimon 1988; Schneider 1990). Even when gravity waves cannot be resolved in the observational data used to initialize weather prediction models, as the models develop mesoscale structure, inertia–gravity waves will begin to play an important role. Although BK intend their speed reduction approach to be used for large-scale applications, in the atmosphere this will limit its usefulness to situations in which the minimum horizontal scales of interest are $O(1000$ km) or greater; with the continually decreasing mesh sizes in both mesoscale and global-scale models, it is not clear that this approach will have broad utility. We believe that in most mesoscale applications, nearly hydrostatic inertia–gravity waves are a "fact of life" and must be resolved accurately within the integration domain, even if it causes numerical difficulties at the lateral boundaries.

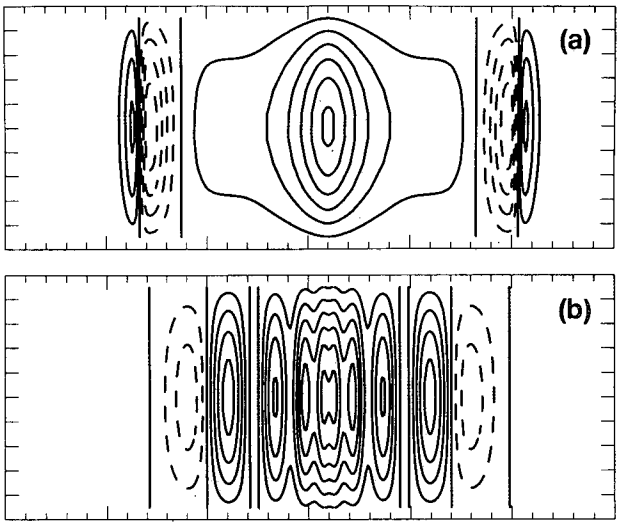

FIG. 5. (a) Perturbation θ at $t = 60\,000$ s for the hydrostatic gravity wave tests, plotted with a contour interval of 0.5×10^{-3} K. (b) The analytic solution for the Browning–Kreiss approximate equations for $\alpha = (1/20)^2$ at $t = 60\,000$ s. The plotted domain is 6000 km × 10 km.

REFERENCES

Bosart, L. F., and A. Seimon, 1988: A case study of an unusually intense atmospheric gravity wave. *Mon. Wea. Rev.*, **116,** 1857–1886.

Browning, G. L., and H.-O. Kreiss, 1986: Scaling and computation of smooth atmospheric motions. *Tellus,* **38A,** 295–313.

——, and A. E. MacDonald, 1993: Incorporating topography into the multiscale systems for the atmosphere and oceans. *Dyn. Atmos. Oceans,* **16,** 119–149.

——, and H.-O. Kreiss, 1994: Splitting methods for problems with different timescales. *Mon. Wea. Rev.,* **122,** 2614–2622.

Cullen, M. J. P., 1990: A test of a semi-implicit integration technique for a fully compressible non-hydrostatic model. *Quart. J. Roy. Meteor. Soc.,* **116,** 1253–1258.

Dudhia, J., 1993: A nonhydrostatic version of the Penn State–NCAR Mesoscale Model: Validation tests and simulation of an Atlantic cyclone cold front. *Mon. Wea. Rev.,* **121,** 1493–1513.

Haltiner, G. J., and R. T. Williams, 1980: *Numerical Prediction and Dynamic Meteorology.* John Wiley and Sons, 477 pp.

Klemp, J. B., and R. Wilhelmson, 1978: The simulation of three-dimensional convective storm dynamics. *J. Atmos. Sci.*, **35,** 1070–1096.

——, and D. K. Lilly, 1980: Mountain waves and momentum flux. *GARP Publ. Ser. 23, Orographic Effects in Planetary Flows,* ICSU/WMO, 450 pp.

Lilly, D. K., J. M. Nichols, R. M. Chervin, P. J. Kennedy, and J. B. Klemp, 1982: Aircraft measurements of wave momentum flux over the Colorado Rocky Mountains. *Quart. J. Roy. Meteor. Soc.,* **108,** 625–642.

Mesinger, F. M., 1977: Forward–backward scheme, and its use in a limited area model. *Contrib. Atmos. Phys.,* **50,** 200–210.

Ogura, Y., and N. A. Phillips, 1962: Scale analysis of deep and shallow convection in the atmosphere. *J. Atmos. Sci.,* **19,** 173–179.

Oliger, J., and A. Sundström, 1978: Theoretical and practical aspects of some initial value problems in fluid dynamics. *SIAM J. Appl. Math.,* **35,** 419–446.

Robert, A. J., 1966: The integration of a low order spectral form of the primitive meteorological equations. *J. Meteor. Soc. Japan,* **44,** 237–245.

Schneider, S. S., 1990: Large-amplitude mesoscale wave disturbances within the intense midwest extratropical cyclone of 15 December 1987. *Wea. Forecasting,* **5,** 533–558.

Skamarock, W. C., and J. B. Klemp, 1992: The stability of time-split numerical methods for the hydrostatic and nonhydrostatic elastic equations. *Mon. Wea. Rev.,* **120,** 2109–2127.

Stobie, J. G., F. Einaudi, and L. W. Uccellini, 1983: A case study of gravity waves—Convective storms interaction: 9 May 1979. *J. Atmos. Sci.,* **40,** 2804–2830.

Tanguay, M., A. Robert, and R. Laprise, 1990: A semi-implicit semi-Lagrangian fully compressible regional forecast model. *Mon. Wea. Rev.,* **118,** 1970–1980.

Tatsumi, Y., 1983: An economical explicit time integration scheme for a primitive model. *J. Meteor. Soc. Japan,* **61,** 269–287.